denatured states, given a force field that accurately describes the characteristics of this limited denatured state. Study of only folded states[20] will be insufficient to solve the folding problem. The key to solving the protein folding problem lies rather in a good understanding of the denatured state.

Methods

The MD simulations were carried out using the GROMOS96 program[18] and the force field 43A1.[19] Aliphatic CH_n groups were treated as united atoms, both in the peptides and the solvents. Periodic boundary conditions were applied in a rectangular or truncated octahedron box. The nonbonded interactions were cutoff at a distance of 1.4 nm, and a Poisson – Boltzmann reaction field force was used to approximate electrostatic interactions beyond the cutoff in water, DMSO, and chloroform. Bond lengths in both peptides and solvents and bond angles in the solvent molecules were kept fixed. The integration time step was 2 fs and systems were kept at constant temperature and pressure (1 atm) by weak coupling to temperature and pressure baths.

The results of the simulations are independent of the various initial structures used because of the relatively long lengths of the simulations. The trajectory structures (at 0.01 ns intervals) of the peptides were clustered into conformations as follows:[8] The number of neighbors (that is, the number of structures satisfying the similarity criterion) was determined for each trajectory structure, with the criterion of similarity between two structures being the positional RMSD value of their main chain atoms. The structure with the highest number of neighbors was then taken as representing the first (most populated) conformation or cluster of structures. After removing the structures belonging to the first cluster from the trajectory, the procedure is repeated to find the second cluster or conformation, and so on.

Received: September 20, 2000 [Z15837]

[1] a) H. J. C. Berendsen, *Science* **1998**, *282*, 642 – 643; b) W. A. Eaton, *Proc. Natl. Acad. Sci. USA* **1999**, *96*, 5897 – 5899; c) N. D. Socci, J. N. Onuchic, P. G. Wolynes, *Proteins Struct. Funct. Genet.* **1998**, *32*, 136 – 158; d) C. M. Dobson, M. Karplus, *Curr. Opin. Struct. Biol.* **1999**, *9*, 92 – 101.

[2] a) A. Fersht, *Structure and Mechanism in Protein Science: A Guide to Enzyme Catalysis and Protein Folding*, Freeman, New York, **1999**; b) D. J. Brockwell, D. A. Smith, S. E. Radford, *Curr. Opin. Struct. Biol.* **2000**, *10*, 16 – 25.

[3] Y. Duan, P. A. Kollman, *Science* **1998**, *282*, 740 – 744.

[4] a) S. J. Hagen, W. A. Eaton, *J. Mol. Biol.* **2000**, *297*, 781 – 789; b) N. A. J. van Nuland, V. Forge, J. Balbach, C. M. Dobson, *Acc. Chem. Res.* **1998**, *31*, 773 – 780.

[5] X. Daura, B. Jaun, D. Seebach, W. F. van Gunsteren, A. E. Mark, *J. Mol. Biol.* **1998**, *280*, 925 – 932.

[6] X. Daura, K. Gademann, B. Jaun, D. Seebach, W. F. van Gunsteren, A. E. Mark, *Angew. Chem.* **1999**, *111*, 249 – 253; *Angew. Chem. Int. Ed.* **1999**, *38*, 236 – 240.

[7] M. Takano, T. Yamato, J. Higo, A. Suyama, K. Nagayama, *J. Am. Chem. Soc.* **1999**, *121*, 605 – 612.

[8] X. Daura, W. F. van Gunsteren, A. E. Mark, *Proteins Struct. Funct. Genet.* **1999**, *34*, 269 – 280.

[9] B. Erman, K. Dill, *J. Chem. Phys.* **2000**, *112*, 1050 – 1056.

[10] Y. Zhou, M. Karplus, *Nature* **1999**, *401*, 400 – 403.

[11] M.-H. Hao, H. A. Scheraga, *J. Mol. Biol.* **1998**, *277*, 973 – 983.

[12] a) E. Alm, D. Baker, *Proc. Natl. Acad. Sci. USA* **1999**, *96*, 11305 – 11310; b) R. L. Baldwin, G. D. Rose, *Trends Biochem. Sci.* **1999**, *24*, 26 – 33.

[13] a) M. Schaefer, C. Bartels, M. Karplus, *J. Mol. Biol.* **1998**, *284*, 835 – 848; b) H. Wang, S.-S. Sung, *J. Am. Chem. Soc.* **2000**, *122*, 1999 – 2009.

[14] a) E. I. Shakhnovich, *Fold Design* **1998**, *3*, R108-R111; b) D. K. Klimov, D. Thirumalai, *J. Chem. Phys.* **1998**, *109*, 4119 – 4125.

[15] F. B. Sheinerman, C. L. Brooks III, *Proc. Natl. Acad. Sci. USA* **1998**, *95*, 1562 – 1567.

[16] G. M. Crippen, Y. Z. Ohkubo, *Proteins Struct. Funct. Genet.* **1998**, *32*, 425 – 437.

[17] a) J. Moult, T. Hubbard, K. Fidelis, J. T. Pederson, *Proteins Struct. Funct. Genet.* **1999**, *37*, 2 – 6, Supplement: Third Meeting on the Critical Assessment of Techniques for Protein Structure Prediction; b) E. Lacroix, T. Kortemme, M. López de la Paz, L. Serrano, *Curr. Opin. Struct. Biol.* **1999**, *9*, 487 – 493.

[18] W. R. P. Scott, P. H. Hünenberger, I. G. Tironi, A. E. Mark, S. R. Billeter, J. Fennen, A. E. Torda, T. Huber, P. Krüger, W. F. van Gunsteren, *J. Phys. Chem. A* **1999**, *103*, 3596 – 3607.

[19] W. F. van Gunsteren, S. R. Billeter, A. A. Eising, P. H. Hünenberger, P. Krüger, A. E. Mark, W. R. P. Scott, I. G. Tironi, *Biomolecular Simulation: The GROMOS96 Manual and User Guide*, Vdf Hochschulverlag AG, Zürich, **1996**.

[20] D. Baker, *Nature* **2000**, *405*, 39 – 42.

[21] C. Peter, X. Daura, W. F. van Gunsteren, *J. Am. Chem. Soc.* **2000**, *122*, 7461 – 7466.

[22] X. Daura, K. Gademann, H. Schäfer, B. Jaun, D. Seebach, W. F. van Gunsteren, *J. Am. Chem. Soc.*, submitted.

[23] R. Bürgi, X. Daura, A. Mark, M. Bellanda, S. Mammi, E. Peggion, W. F. van Gunsteren, *J. Peptide Res.*, in press.

[24] C. Santiveri, M. A. Jiménez, M. Rico, W. F. van Gunsteren, X. Daura, personal communication.

Electronic Insight into an Antithrombotic Agent by High-Resolution X-Ray Crystallography**

Ralf Flaig, Tibor Koritsánszky, Rainer Soyka, Ludger Häming, and Peter Luger*

In medicinal chemistry it is generally accepted that steric and electronic properties play a dominant role in drug – target recognition processes. Molecular activity, similarity, and recognition, which are ambiguously defined properties, are therefore most often screened in terms of their relationship to a definite and readily accessible property, the molecular structure. However, all of these properties can be deduced unambiguously from the distribution of the electronic charge,

[*] Prof. Dr. P. Luger, Dr. R. Flaig
Institut für Chemie/Kristallographie
der Freien Universität Berlin
Takustrasse 6, 14195 Berlin (Germany)
Fax: (+49) 30-838-53464
E-mail: luger@chemie.fu-berlin.de
Prof. Dr. T. Koritsánszky
Department of Chemistry, University of the Witwatersrand
Private Bag 3, WITS 2050, Johannesburg (South Africa)
Dr. R. Soyka
Research and Development, Boehringer Ingelheim Pharma KG
Birkendorfer Strasse 65, 88397 Biberach (Germany)
Dr. L. Häming
Bruker Analytical X-ray Systems
Östliche Rheinbrückenstrasse 50, 76187 Karlsruhe (Germany)

[**] This work was funded by the Bundesministerium für Bildung, Wissenschaft, Forschung und Technologie (BMBF), Bonn (Germany) (grant no. 05 SM8KEA0) and by the Fonds der Chemischen Industrie, Frankfurt (Germany).

which is a physical property that can be observed and derived from the first principles of quantum mechanics.[1, 2] Despite recent dynamic advances in theoretical methods, the modeling of drug–receptor interactions at the electronic level is not yet a feasible approach. Owing to the complexity of biochemical systems and to the lack of information on the receptor site, practical models are limited to drug molecules with properties that are established, at most, at the semiempirical level of theory.

The charge or electron density $\rho(\boldsymbol{r})$ can be obtained theoretically from high level ab initio quantum chemical calculations and also experimentally from a high-resolution X-ray diffraction experiment at low temperature ($T \leq 100$ K). The charge density extracted from the X-ray diffraction data of a crystalline sample does not correspond to the pure quantum state. Although the applied pseudoatom formalism[3] is a density model which is formally equal to a one-center representation of $\rho(\boldsymbol{r})$, it does not allow for the reconstruction of the wave function, hence, orbitals, for example, are not observable in the deformation density.[4, 5]

The rationalization of the experimental charge density has been made possible through their comparison with theoretical densities. In this respect topological analyses have played a major role.[2] Such studies have demonstrated that the experimental density is homologous not only to that derived from the ground-state periodic wave function but also to that calculated for the isolated molecule with the experimental geometry.[6–8] The experimental charge density obtained after multipole refinement[3] is affected by experimental errors and model inadequacies. The quality of the theoretical counterpart, on the other hand, depends primarily on the approximations involved and the basis set used in the calculation. The comparison of experimental and theoretical bond topological descriptors for chemically analogous bonds reveals that the spread of these parameters, as changing conditions, is narrower for the former than for the latter method.[9]

By making use of recent technical developments in X-ray crystallography[10–12] we were able to investigate the charge density[13] and related topological properties of an antithrombotic drug molecule of more than 50 atoms. The comparison of experimental and theoretical properties suggests that those extracted from X-ray data, and thus referring to the crystalline environment, are substantially better suited to simulate physiological conditions than those calculated for the isolated molecule.

Terbogrel (Figure 1) is a new antithrombotic agent which is in the course of clinical development. It has recently been introduced as the first compound with a guanidine moiety to combine antagonism to the thromboxane A_2 receptor and synthase inhibition.[14, 15] The experimental results presented here are based on an X-ray data set of almost 220 000 reflections up to a resolution of $d = 0.4$ Å that were collected in 5 days by using area detection.[16] This is to be compared with approximately 200 days of exposure time that would have been needed for the corresponding experiment performed with conventional scintillation detection, or to over 85 days of CPU time on a SGI Origin 2000 (R10000 processor) that would be needed to calculate the corresponding results for the isolated molecule at the

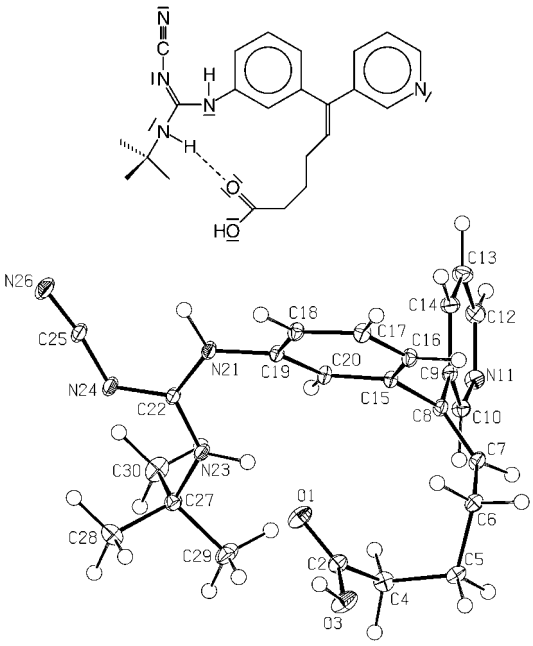

Figure 1. Chemical formula of Terbogrel and its molecular structure as obtained by this X-ray study (ORTEP representation,[23] the displacement ellipsoids are plotted at a 50% probability level).

HF/6-311++G(3df,3pd) level of theory with the GAUSSIAN94 program package.[17] The resulting intensity data were interpreted in terms of the Hansen and Coppens multipole formalism,[3] which allows the modeling of an aspherical distribution of electron density. The multipolar refinement with the program package XD[18] led to a crystallographic agreement factor of 1.8%. This value shows the excellent quality of the crystal and diffraction intensities. Hence, even the use of a conventional X-ray source is suited for these types of investigations.

From the analytic charge density obtained it is possible to perform a topological analysis according to Baders theory of "atoms in molecules".[2] This analysis provides the definition of molecular structure, an atomic partitioning of the molecule, and the characterization of atomic interactions in terms of local topological indices—such as the value of the electron density $\rho(\boldsymbol{r}_b)$ and its Laplacian function $\nabla^2\rho(\boldsymbol{r}_b)$ at the bond critical point (BCP, located at $\boldsymbol{r}_b$, where $\nabla\rho(\boldsymbol{r}_b) = 0$), as well as the bond ellipticity ε[19] (see also Table 1).

Table 1 shows a comparison of theory and experiment in terms of quantitative bond topological data for various C–N bonds in the guanidine group, the cyano group, and the pyridine ring of Terbogrel (Figure 1). The weakest bond strength, as given by $\rho(\boldsymbol{r}_b)$, is found for the bond N23–C27 with an experimental value of 1.76(2) e Å^{-3}, which indicates an almost pure single bond. This result is supported by the bond ellipticity which is close to zero and shows a cylindrical density distribution along the bond. A $\rho(\boldsymbol{r}_b)$ value of 2.05 e Å^{-3} for the bond N21–C19 is lower and higher, respectively, than that expected for a double and single bond, which suggests there is conjugation with the phenyl ring. The topological equivalence of the N11–C10 and N11–C12 bonds may be attributable to the aromatic character of the pyridine ring. High charge concentrations are found for the formally single

  1433-7851/01/4002-0356 $ 17.50+.50/0 *Angew. Chem. Int. Ed.* **2001**, *40*, No. 2

Table 1. Bond topological indices for the various N–C bonds.[a]

Bond	$\rho(r_b)$	$\nabla^2\rho(r_b)$	d	ε
N23–C27	1.61	– 10.3	0.996	0.02
	1.65	– 14.3	0.986	0.03
	1.76(2)	– 8.8(1)	0.831	0.03
N21–C19	1.91	– 15.7	0.941	0.05
	1.97	– 20.8	0.931	0.04
	2.05(2)	– 13.8(1)	0.799	0.10
N21–C22	2.17	– 23.4	0.895	0.05
	2.24	– 28.9	0.886	0.10
	2.35(2)	– 16.4(1)	0.758	0.12
N11–C10	2.30	– 19.9	0.883	0.10
	2.37	– 26.2	0.874	0.13
	2.47(2)	– 21.2(1)	0.755	0.14
N11–C12	2.29	– 19.4	0.885	0.08
	2.37	– 25.9	0.876	0.12
	2.51(1)	– 22.3(1)	0.763	0.13
N24–C22	2.42	– 30.5	0.838	0.14
	2.50	– 34.4	0.823	0.17
	2.53(2)	– 20.9(1)	0.725	0.08
N24–C25	2.46	– 30.1	0.827	0.04
	2.52	– 32.9	0.827	0.04
	2.60(2)	– 18.7(1)	0.726	0.04
N23–C22	2.36	– 27.2	0.868	0.13
	2.44	– 32.9	0.858	0.18
	2.62(2)	– 24.3(1)	0.742	0.19
N26–C25	3.15	– 9.6	0.757	0.03
	3.25	– 12.3	0.760	0.03
	3.54(2)	– 35.5(1)	0.685	0.08

[a] $\rho(r_b)$ [e Å^{-3}] and $\nabla^2\rho(r_b)$ [e Å^{-5}] are calculated from the corresponding bond critical point (BCP); d [Å] gives the distance of the BCP from the first listed atom; and the bond ellipticity ε indicates the aspherical nature of the charge in the bond.[19] For each bond the first line corresponds to HF/6-311++G(d,p), the second line to HF/6-311++G(3df,3pd), and the third line to experimental results.

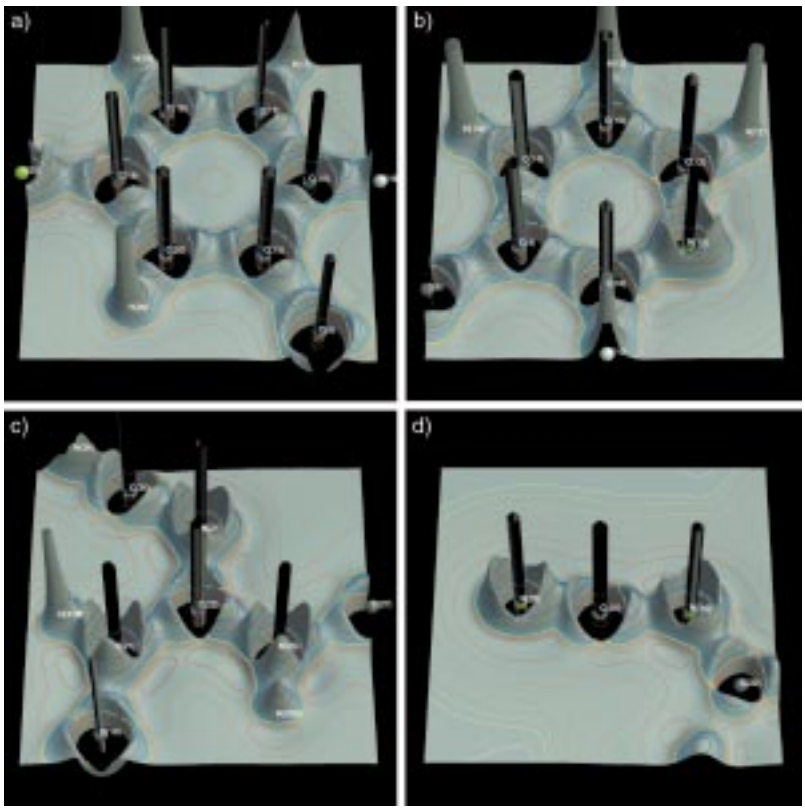

Figure 2. Comparison of the negative Laplacian distribution in four different molecular sections: a) the phenyl ring, b) the pyridine ring, c) the guanidine group, d) the terminal cyano group. The Laplacian function is a very sensitive indicator of local charge accumulations ($\nabla^2\rho(r) < 0$) or depletions ($\nabla^2\rho(r) > 0$). The saddle-shaped features in the bonding regions are typical indicators of the charge concentrations on a covalent bond. The lone pairs on the nitrogen atoms are also all signaled.

bonds N23–C22 and N24–C25 in the guanidine residue. In terms of their $\rho(r_b)$ values, the other two bonds to C22 appear to have strong double bond character. The overall trend found here can be rationalized on the basis of the resonance forms depicted in Scheme 1. The bond orders of the different C–N bonds, as revealed by the $\rho(r_b)$ values, suggest the resonance forms **4** and **6** to have considerable weight.

The Laplacian distribution of the charge density yields valuable chemical information on the reactive sites of the molecule and on the sites where intermolecular interactions are favored. Figure 2 displays this function in a few selected molecular planes, and shows features such as bonded valence shell charge concentrations (VSCCs, with local maxima at $-\nabla^2\rho(r_b)$) on all the covalent bonds and nonbonded VSCCs in the lone-pair regions of the nitrogen and oxygen atoms. Figure 3 displays the zero-Laplacian isosurface (the reactive surface) and shows a high depletion of the VSCC at C2 and C22. These two atoms are therefore the most likely sites for a nucleophilic attack. On the basis of the nonbonded VSCCs

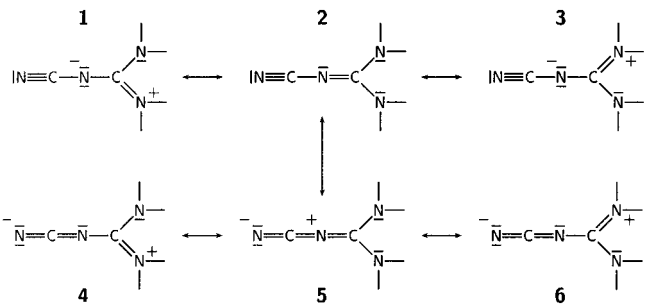

Scheme 1. Different resonance forms of the guanidine fragment. On the basis of the results from the topological analysis the resonance forms **4** and **6** have considerable weight.

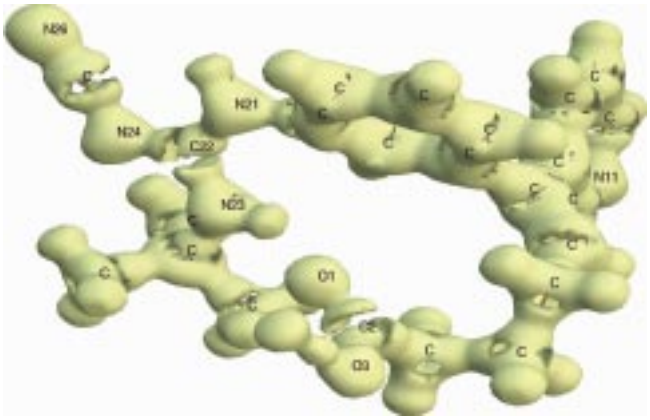

Figure 3. Zero-Laplacian isosurface ($\nabla^2\rho(r) = 0$, reactive surface). The labels for the H atoms are omitted. The VSCC at atoms C2 and C22 is reduced, as shown by the open regions in this surface. These are the most likely sites for nucleophilic attack.

  1433-7851/01/4002-0357 $ 17.50+.50/0

(Table 2), the oxygen atoms, as well as atoms N11 and N26 appear to be the most likely sites for an electrophilic attack since $\nabla^2\rho(\boldsymbol{r}_b)$ shows the most negative values, and hence local charge concentration at these sites. This result is in excellent

Table 2. Nonbonded valence shell charge concentrations.[a]

Atom	$\rho(\boldsymbol{r}_b)$		$\nabla^2\rho(\boldsymbol{r}_b)$		R	
N11	4.02	4.08	− 74.1	− 83.9	0.388	0.389
N21	3.27	–	− 39.9	–	0.411	–
	3.28	–	− 40.4	–	0.411	–
N23	3.20	–	− 37.7	–	0.413	–
	3.20	–	− 37.6	–	0.414	–
N24	3.65	3.64	− 57.1	− 57.4	0.398	0.397
N26	3.63	3.85	− 60.2	− 70.5	0.396	0.391
O1	6.27	6.39	− 124.0	− 133.1	0.344	0.340
	6.31	6.50	− 125.1	− 133.8	0.344	0.339
O3	6.33	6.77	− 124.2	− 152.5	0.343	0.336
	–	6.30	–	− 129.5	–	0.342

[a] In each column the entries on the left correspond to the theoretical calculation (HF/6-311 ++ G(3df,3pd)), and the entries on the right to the experiment. $\rho(\boldsymbol{r}_b)$ [e Å^{-3}] and $\nabla^2\rho(\boldsymbol{r}_b)$ [e Å^{-5}] are the values found at the (3,+3) critical point of the Laplacian. R [Å] is the distance from the corresponding atom to this point.

agreement with that derived from the wave function. On the other hand, the analysis of the experimental $-\nabla^2\rho(\boldsymbol{r}_b)$ function reveals the lack of (3, − 3) critical points at the N21 and the N23 sites. This finding also supports the suggestion that the nonbonded electrons of these atoms are, to some extent, involved in the bonding as suggested by the resonance forms **4** and **6**.

The electrostatic potential (EP), which can be derived directly from the electron density, is an analytical tool which is used extensively to predict the reactive behavior of chemical systems and to study biological recognition processes, such as drug – receptor or enzyme – substrate interactions. Figure 4 displays positive (blue) and negative (red) isopotential surfaces of the EP derived from the monomolecular charge density extracted from the crystal field according to the method of Su and Coppens,[20] and compared to that calculated from the HF/6-311 ++ G(d,p) wave function. Both maps show distinct regions of negative potential that are especially pronounced at the cyano-substituted guanidine residue and, to a lesser extent, at the pyridine nitrogen and carboxylate oxygen atoms. These features are considerably enhanced in the experimental potential and indicates the polarization effects of the crystal field. The enlargement of the dipole moment on going from the isolated molecule (11.2 D, HF/6-311 ++ G(3df,3pd)) to that in the crystalline environment (21.9(16) D) has the same origin. These observations are in line with several results published recently on experimental electronic properties.[21, 22]

The experimental EP extracted from the crystalline state can be assumed to be better suited for the simulation of a physiological situation, which are characteristic of drug – receptor interactions, than the potential calculated from an isolated stationary state. This occurs because it includes effects of intermolecular interactions arising from a given crystal packing in which molecular recognition is realized to a high degree. To obtain comparable results theoretically,

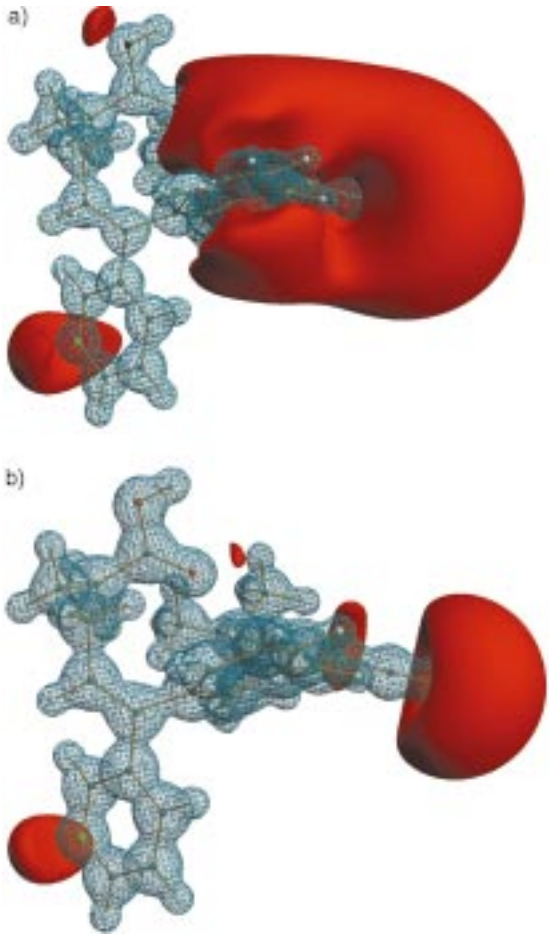

Figure 4. Representation of the isosurface of the electrostatic potential: a) Experimental, extracted from the crystal field by the method of Su and Coppens,[20] b) calculated from HF/6-311 ++ G(d,p) wave function for the isolated molecule. The values of the isosurface in both representations are: red = − 0.1 e Å^{-1}, blue = + 1.0 e Å^{-1}.

calculations need to be carried out on periodic systems, which is hardly feasible with current CPU power and definitely impossible for larger systems. This fact encourages the use of experimentally derived electronic properties in the modeling of biochemical processes since purely geometric considerations are certainly not sufficient for their description. Only steric and electronic complementarity will lead to a successful drug – receptor interaction, hence the accurate determination of the electronic charge density serves as a basis for a better understanding of such interactions. Since this study has proven that charge-density work on medium-sized drug molecules can be performed even with common laboratory equipment in a short time, this method has the potential to improve drug-finding processes.

Received: July 14, 2000 [Z 15449]

[1] P. Hohenberg, W. Kohn, *Phys. Rev. B* **1964**, *136*, 864.
[2] R. F. W. Bader, *Atoms in Molecules: A Quantum Theory*, Clarendon, **1990**.
[3] N. K. Hansen, P. Coppens, *Acta Crystallogr. Sect. A* **1978**, *34*, 909.
[4] J. M. Zuo, M. Kim, M. O'Keeffe, J. C. H. Spence, *Nature* **1999**, *401*, 49.
[5] C. J. Humphreys, *Nature* **1999**, *401*, 21.

  1433-7851/01/4002-0358 $ 17.50+.50/0

[6] C. Gatti, R. Bianchi, R. Destro, F. Merati, *THEOCHEM* **1992**, *255*, 409.
[7] T. Koritsánszky, J. Buschmann, P. Luger, *J. Phys. Chem.* **1996**, *100*, 10547.
[8] C. Gatti, V. R. Saunders, C. Roetti, *J. Chem. Phys.* **1994**, *101*, 10686.
[9] R. Flaig, T. Koritsánszky, J. Janczak, H.-G. Krane, W. Morgenroth, P. Luger, *Angew. Chem.* **1999**, *111*, 1494; *Angew. Chem. Int. Ed.* **1999**, *38*, 1397.
[10] T. Koritsánszky, R. Flaig, D. Zobel, H.-G. Krane, W. Morgenroth, P. Luger, *Science* **1998**, *279*, 356.
[11] B. B. Iversen, F. K. Larsen, A. A. Pinkerton, A. Martin, A. Darovsky, P. A. Reynolds, *Acta Crystallogr. Sect. B* **1999**, *55*, 363.
[12] S. Dahaoui, C. Jelsch, J. A. K. Howard, C. Lecomte, *Acta Crystallogr. Sect. B* **1999**, *55*, 226.
[13] P. Coppens, *X-Ray Charge Densities and Chemical Bonding*, Oxford University Press, Oxford, **1997**.
[14] R. Soyka, B. D. Guth, H. M. Weisenberger, P. Luger, T. H. Müller, *J. Med. Chem.* **1999**, *42*, 1235.
[15] J. Wouters, F. Durant, B. Masereel, *Bioorg. Med. Chem. Lett.* **1999**, *9*, 2867.
[16] Crystallographic data: $C_{23}O_2N_5H_{27}$, $M_r = 405.49$, monoclinic $P2_1/a$, $a = 14.832(2)$, $b = 10.097(1)$, $c = 15.599(2)$ Å, $\beta = 113.55(1)^\circ$, $V = 2141.52$ Å^3, $Z = 4$, $\rho_{calcd} = 1.258$ g cm^{-3}, $Mo_{K\alpha}$ radiation ($\lambda = 0.7107$ Å), $T = 100$ K, Bruker-AXS SMART diffractometer, CCD area detector, 219870 measured reflections, 39356 unique, $d = 0.4$ Å, $\sin\theta/\lambda_{max} = 1.25$ Å^{-1}, $R(F) = 0.0236$, $R_w(F) = 0.0180$ after multipole refinement, hexadecapolar for C, N, O, one quadrupole, otherwise dipoles for H. Crystallographic data (excluding structure factors) for the structures reported in this paper have been deposited with the Cambridge Crystallographic Data Centre as supplementary publication no. CCDC-147443. Copies of the data can be obtained free of charge on application to CCDC, 12 Union Road, Cambridge CB2 1EZ, UK (fax: (+44) 1223-336-033; e-mail: deposit@ccdc.cam.ac.uk).
[17] Gaussian 94, Revision E.2, Gaussian, Inc., Pittsburgh, PA, **1995**.
[18] T. Koritsánszky, S. Howard, T. Richter, Z. W. Su, P. R. Mallinson, N. K. Hansen, *XD—A Computer Program Package for Multipole Refinement and Analysis of Electron Densities from Diffraction Data. User Manual*, Freie Universität Berlin, **1995**.
[19] The ellipticity ε is defined by $(\lambda_1/\lambda_2) - 1$, with λ_1 and λ_2 being the two principal curvatures of $\rho(\boldsymbol{r})$ at a BCP, and is a measure of the aspherical nature of the charge in a chemical bond.
[20] Z. Su, P. Coppens, *Acta Crystallogr. Sect. A* **1992**, *48*, 188.
[21] J. Gao, C. Alhambra, *J. Am. Chem. Soc.* **1997**, *119*, 2962.
[22] M. A. Spackman, *Chem. Rev.* **1992**, *92*, 1769.
[23] M. N. Burnett, C. K. Johnson, *ORTEP-III*, *Oak Ridge Thermal Ellipsoid Plot Program for Crystal Structure Illustrations*, Oak Ridge National Laboratory, **1996**.

Polyol-Mediated Preparation of Nanoscale Oxide Particles**

Claus Feldmann* and Hans-Otto Jungk

Nanoscale oxide particles with a mean particle diameter of 30 to 300 nm are gaining increasing technical importance for classic areas of application such as catalysts, passive electronic components, or ceramic materials.[1] However, they also contribute in an essential way to the realization of completely new concepts such as transparent solar cells[2] or photonic crystals.[3] In addition, they play an important role in the selective surface modification (e.g. passivation, hardening, coloration) of various substrates in the form of coatings.[4] With regard to all of the applications mentioned, in addition to the particle size a low degree of agglomeration and a monodisperse size distribution are desirable to enable a homogeneous arrangement of particles in thin films or as coatings. The polyol method applied herein provides a promising preparative approach to such oxide particles.

The polyol method was initially described for the preparation of elemental metals and alloys,[5] in which the reducing properties of a high-boiling alcohol (e.g. glycerol, glycol) towards a suitable metal precursor were utilized. With regard to oxidic materials, only a few insights have been gained so far, namely for ZnO, Fe_2O_3, $CoAl_2O_4$, and Bi_2O_3.[6] Our investigations show that the polyol method, which can also be understood as a sol–gel process carried out at elevated temperatures in the case of oxides, is suitable for the preparation of a host of binary and ternary oxides.

By heating suitable metal salts and a defined amount of water in diethylene glycol (DEG), suspensions of various materials are obtained in a simple manner (Figure 1, Table 1). These oxide particle suspensions are colloidally stable and can contain up to 20 wt % of solids. A detailed characterization of the oxide particles obtained is exemplified for Cu_2O, TiO_2,

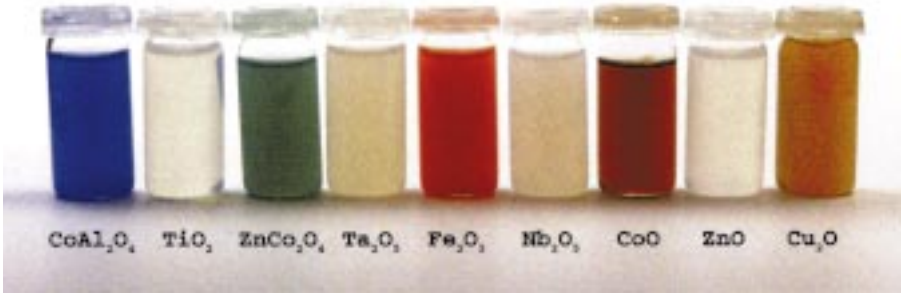

Figure 1. Various oxide particle suspensions in DEG.

[*] Dr. C. Feldmann, H.-O. Jungk
Philips GmbH
Forschungslaboratorien
52066 Aachen (Germany)
Fax: (+49) 241-6003-465
E-mail: claus.feldmann@philips.com

[**] We thank Jacqueline Merikhi and Gerd Much for carrying out the scanning electron microscopy (SEM) and the atomic force microscopy (AFM) investigations, respectively.

  1433-7851/01/4002-0359 $ 17.50+.50/0